Master's Thesis

Evaluating sensor accuracy and repeatability in gasketed plate heat exchangers

Author:
Nils Engman

Supervisor:
Anders Nyander (Alfa Laval)

Co-supervisor
Henrik Kockum (Alfa Laval)

Supervisor:
Christian Antfolk (LTH)

Examiner:
Johan Nilsson (LTH)

Lund University

Faculty of Engineering LTH
Department of Biomedical Engineering
Electrical Measurements

June 29, 2023

LUND UNIVERSITY

Abstract

Faculty of Engineering LTH

Department of Biomedical Engineering

Master of Science

Evaluating sensor accuracy and repeatability in gasketed plate heat exchangers

by Nils Engman

Alfa Laval has connected sensors to their gasketed plate heat exchangers (GPHE) to extend their customer service offering. To develop this service further the flow through the GPHE is needed. In this thesis, the objective was to evaluate an inexpensive flow switch and two sensor kits that measure pressure and temperature. The sensors were assessed by installing them on GPHEs in Alfa Laval's lab and running seven test sessions. The flow switch performed well but experienced "jumps" in the output and a temperature dependence that could be compensated for through multiple regression. The sticker sensors temperature measurements were accurate, but more calibration is needed to get the pressure. Regarding the in-house kit, the pressure measurements were reliable, but the temperature measurements suffer from lag and thermal inertia. The thesis has offered valuable insight that will propel Alfa Laval's pursuit of a cost-effective way of measuring the flow and improving their service capabilities.

Acknowledgements

I would like to express my gratitude to my supervisor and co-supervisor at Alfa Laval, Anders Nyander and Henrik Kockum, for their guidance and support throughout this research endeavor. Their valuable input and expertise have greatly contributed to the development of this thesis. I appreciate their commitment and feedback, which have significantly enhanced the quality of my work. Anders Dahl and Milos Milovancevic have given me above and beyond lab assistance for which I am very grateful. I also extend my thanks to my academic supervisor, Christian Antfolk, for his valuable guidance and support.

Contents

Chapter 1

Introduction

Alfa Laval is a global company established in Sweden in 1883. They provide products in the areas of separation, fluid handling and heat transfer. They offer four main types of heat exchangers (HE): plate heat exchangers, air-cooled heat exchangers, scraped surface heat exchangers and tubular heat exchangers. Heat exchangers are used everywhere, from huge installations in nuclear power plants and oil refineries to data centres and more. In this master thesis, I will work with a specific type of plate heat exchanger called a gasketed plate heat exchanger (GPHE). In contrast to other plate HE, GPHEs are held together using tightening bolts and the plates are sealed using gaskets. They are manufactured and developed in Lund. A thorough description of GPHEs and their working principles is given in chapter 2. Up until recently, Alfa Laval's GPHEs did not contain or come with any electrical equipment. But, an in-house sensor kit has been developed that enables an entirely new service model. Alfa Laval is continuously improving their service capabilities, this model is part of an ongoing process of digitalization and service improvement. By subscribing to this service, customers get access to an Alfa Laval cloud page. On this page, the customer can view information about their heat exchangers, such as the uptime, downtime, time until maintenance and possible carbon-dioxide savings.

Service was, and still is, mostly carried out based on the time since the last service. Shifting to an Internet of Things (IoT) solution comes with a few benefits. By installing sensors and connecting these

to the cloud, Alfa Laval can collect information about the state of the GPHEs and notify the customer when service needs to be done. By doing so, the customer can avoid uneconomic operation or even heat exchanger failure which in some cases could be very costly. One example could be a dairy process, where the HE is necessary to keep the dairy product at the right temperature to keep it from spoiling. Consequently, the value for the customer is mostly in the security of operations. However, if the prediction is precise, let us say Alfa Laval could predict the time for service at a precise week, then the customer could plan for the service or purchase of a new heat exchanger in such a way that it would not disturb their operation. There are more benefits to the cloud solution. An overview of the CO_2-emissions that are emitted due to the reduced efficiency caused by fouling in the heat exchanger can be shared with the customers. Hopefully, this feature could lead to more customers ordering the service earlier or exchanging their heat exchangers, generating more revenue for Alfa Laval and less CO_2-emissions.

1.1 Purpose

To generate the information on the customers cloud page, sensors are installed on their GPHEs. The sensor kit currently available to Alfa Laval customers measures two parameters, temperature & pressure, at each inlet and outlet port. To improve the accuracy of the information provided to the customers the flow in the heat exchanger is required. Flow sensors are usually expensive and difficult to install. Thus, the purpose of this thesis is to test inexpensive sensors with the goal of improving Alfa Laval's service capabilities.

1.2 Research objectives

The objective of this thesis is two fold. The primary objective is the evaluation of an inexpensive flow switch for flow measurements. The second objective is to evaluate the reliability and accuracy of an in-house sensor kit and a sticker sensor kit.

1.3 Delimitations

The main delimitation of the thesis is the access to data. Since GPHEs come in many sizes and configurations it will not be possible to test a generalized model. A more realistic goal is to identify sensors with potential and generalized models that can be built upon when more data are available.

1.4 Method

To evaluate the sensors, they were installed on GPHEs in Alfa Laval's lab. The GPHEs could then be run while controlling the temperature, flow and pressure. data were collected from the evaluated sensors and from the sensors permanently installed in the lab which served as reference data. In total, seven test sessions were performed, each lasting a couple of hours. To get as much value as possible, the sessions were planned to test the limits of the sensors e.g. sensitivity, resolution and drift. After the data had been collected it was visualized and analysed. The data from the flow switch was fitted to the reference data using simple and multiple regression.

Chapter 2

Background

2.1 Gasketed plate heat-exchangers

Gasketed plate heat-exchangers have three main parts: (1) the two covers, one in front and one in the back; (2) the plates and (3) the gaskets. Most GPHEs are designed for heat exchange between two media. One media is cold and the other is hot, as depicted in figure 2.1 by blue (cold) and red (hot) arrows. There is one inlet and outlet for each media. In a counter-current GPHE the hot and cold inlets are vertically opposite each other, one on the top and one on the bottom. Once the media have entered the heat exchanger through the connections in the front cover they encounter the plates. The plates are pushed together between the covers and the media flows in between the plates. The gaskets between the plates make sure that there is no leakage. One plate does not encapsulate the media on its own, the channels that the media flow through are formed between the plates that are held together. The plates are installed with alternating vertical direction so that cold media flows in the first channel, then the hot media and so on, it could also start with the hot media, the point being that they alternate. The actual exchange of heat occurs in the channels between the plates and through the plates that separate the media. The plates are divided into three zones, the adiabatic zone, the distribution zone and the heat transfer zone. The adiabatic zone is where the media enters the channel, the distribution zone comes next and aims to distribute the media evenly across the

width of the channel. Heat transfer does not occur in the adiabatic zone since there is no media on the other sides of the plates.

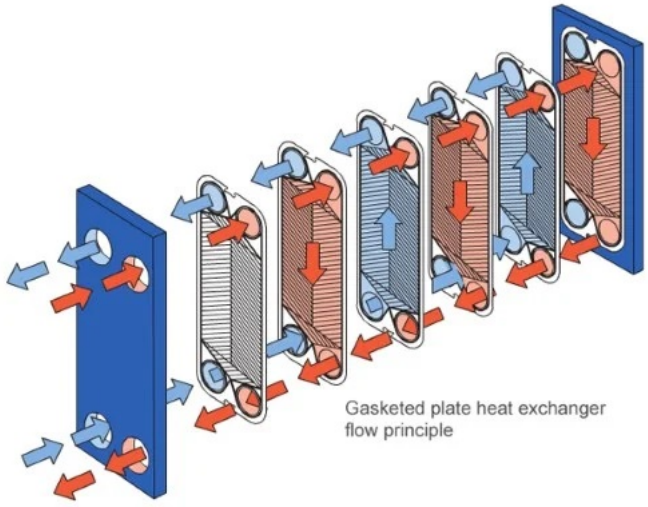

FIGURE 2.1: An overview of the flow principle of a GPHE from Alfa Laval. Source: (Laval, n.d.)

The part of the GPHE where the media enters is called the connection, it includes: the flange that sits between the cover plate and the pipe connecting the heat exchanger and the holes in the cover plates. The "hole" that is formed when the plates are pushed together can be seen as an internal pipe with exit or entry holes for the channels between the plates. This "pipe" section is called the port. A schematic of the terminology can be seen in figure 2.2.

Gasketed plate heat exchangers are usually made of stainless steel but can be made in several different materials depending on the application, the same goes for the gaskets even though they are usually made of NBR or EPDM.

To understand how a heat exchanger work we must first go through some basic thermodynamic theory. Heat is transported through three processes, conduction, convection and radiation. In the case of heat

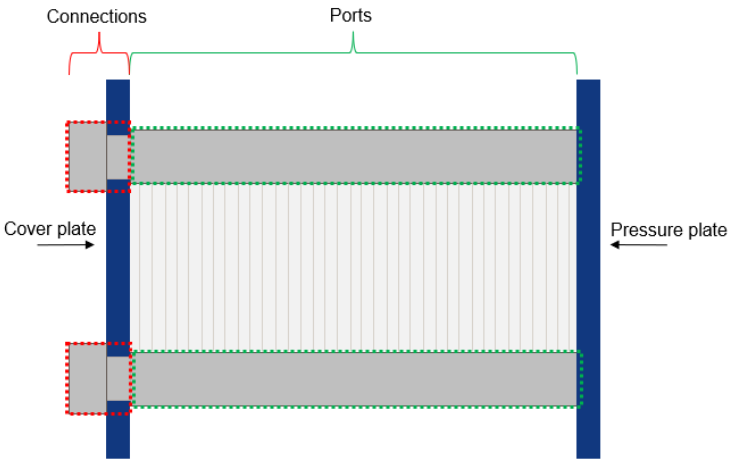

FIGURE 2.2: A schematic showing the connections and ports of a GPHE. In the figure, the GPHE is viewed from the side

exchangers the heat transferred by radiation will be marginal in comparison to the other two processes, thus I will not go into further detail about radiation (Hewitt et al., 1994). When atoms and molecules collide vibrations are transmitted, this is a form of heat transport called conduction (Hewitt et al., 1994). Convection, on the other hand, is based on the bulk movement of fluid (Hewitt et al., 1994). The degree of conduction and convection is dependent on the temperature gradient, the type of media and the flow profile. For example, if there is a lot of turbulence, the media will be mixed and therefore also the heat. Given that turbulence is such an important fluid motion it is imperative to understand what influences the turbulence.

Turbulence is dependent on the properties of the liquid such as viscosity; in a high viscosity liquid there is a lot of internal friction, it feels thicker because there is a high resistance to layers of the liquid sliding past each other. An illustrative real-life example is the comparison of oil and water. Oil has a high viscosity and will therefore experience less turbulence than for example water, which is less viscous, given the same volume flow rate. The Reynolds number is often used to determine whether the flow is turbulent or moving in

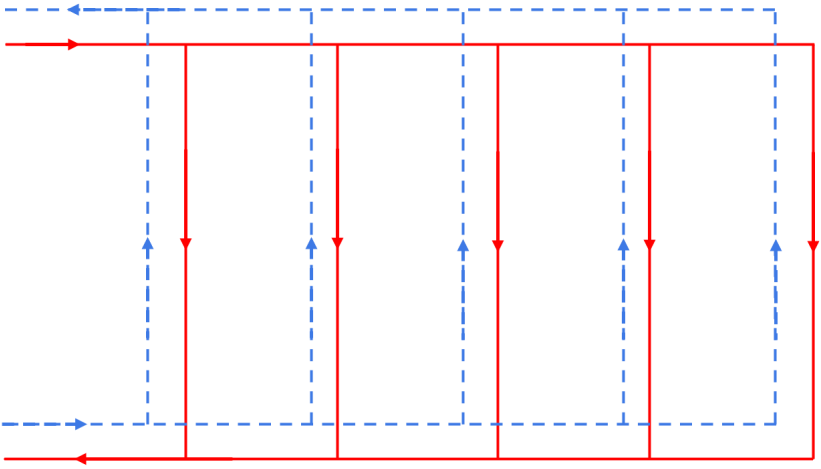

FIGURE 2.3: A schematic showing the flow arrangement of a plate heat exchanger with a counter-current flow profile and ten channels, five in each direction

smooth layers which constitutes laminar flow. The Reynolds number is shown in equation 2.1 (Batchelor and Batchelor, 1967, p.212). In the equation, the effect of the previously mentioned flow conditions are included.

$$Re = \frac{\rho v L}{\mu} \tag{2.1}$$

The Reynolds number is dependent on the fluid density ρ, viscosity μ, the characteristic velocity v and length L. A higher Reynolds number means that the fluid flow is more turbulent than flow with a lower number. The transition region between laminar flow and turbulent flow is at a Reynolds number of around 2100 (Guo and Ghalambor, 2014).

2.1.1 Heat Balance and rate of heat transfer

The heat balance is described by equation 2.2, 2.4 and 2.4. The heat flow rate is equal to the mass flow rate, m, times the enthalpy

change, Δh. Side 1 has a negative heat flow rate and side 2 has a positive. The enthalpy change is equal to the product of the average heat capacity $\langle c_p \rangle$ and the temperature difference on each side of the heat exchanger i.e. side 1 and side 2. In a GPHE the internal area is much larger than the area exposed to the surroundings. The loss of heat to the surroundings can therefore be disregarded (Sundén and Manglik, 2007).

$$\text{Side } 1 : 0 = m_1 \Delta h_1 + Q \tag{2.2}$$

$$\text{Side } 2 : Q = m_2 \Delta h_2 \tag{2.3}$$

$$Q = m_1 \langle c_p \rangle_1 (T_{\mathrm{h,i}} - T_{\mathrm{h,o}}) = m_2 \langle c_p \rangle_2 (T_{\mathrm{c,o}} - T_{\mathrm{c,i}}) \tag{2.4}$$

Where h is the enthalpy and c_p is the heat capacity. The rate of heat transfer, Q, is equal to the overall heat transfer coefficient, U, multiplied with the heat transfer area and the logarithmic mean temperature difference (LMTD), ΔT_m (Sundén and Manglik, 2007).

$$Q = UA\ \Delta T_m = UA\ LMTD \tag{2.5}$$

The area of a GPHE is dependent on the size of the device i.e. the number of plates, and the length and width of the plates. The coefficient U is much harder to quantify, it can be viewed as a series of resistances much like an electric circuit. Equation 2.6 shows the coefficient U as a function of the heat transfer coefficients h_{h}, h_{c}, the plate thickness δ_{w}, the thermal conductivity of the plate wall λ_{w} as well as the fouling resistances, $R_{f,\mathrm{h}}$ and $R_{f,\mathrm{c}}$, for the hot and cold sides respectively (Sundén and Manglik, 2007).

$$\frac{1}{U} = \frac{1}{h_{\mathrm{h}}} + \frac{1}{h_{\mathrm{c}}} + \frac{\delta_{\mathrm{w}}}{\lambda_{\mathrm{w}}} + R_{f,\mathrm{h}} + R_{f,\mathrm{c}} \tag{2.6}$$

The heat transfer coefficients are specific for each channel, fluid and fluid velocity. Due to this complex character, they can only be determined experimentally.

2.1.2 Logarithmic mean temperature difference

In equation 2.5 we could see that the heat flow rate is proportional to the LMTD. Thus, if we want to maximize heat transfer, we want a high LMTD. The calculation of the LMTD is shown in equation 2.7, where ΔT_1 is the temperature difference between the hot inlet and the cold outlet, ΔT_2 hot outlet and cold inlet (Sundén and Manglik, 2007).

$$\Delta T_m = \frac{\Delta T_1 - \Delta T_2}{\ln(\Delta T_1 / \Delta T_2)} \tag{2.7}$$

If the goal is to maximize the LMTD it is better to have an even difference in temperature across the whole GPHE than to have a large difference on one end and a smaller difference on the other the end (Sundén and Manglik, 2007). For a GPHE, the design choices counter-current and co-current have a large impact on the LMTD. The counter-current design has an even temperature difference GPHE while the co-current design has a large temperature difference on one end but not the other. A counter-current flow arrangement was shown in figure 2.1 and 2.3. The temperature distribution for a counter-current flow arrangement is shown in figure 2.4.

2.1.3 Pressure Drop

When choosing a GPHE the user usually considers the cost of the GPHE as well as the cost of pumping the media. With a higher pressure drop more energy is needed to run the pumps. The pressure drop is defined as the pressure drop through the heat-exchanger, from the inlet to the outlet. When selling a GPHE Alfa Laval usually have a certain limit on the pressure drop, for example 100kPa.

Currently, the pressure drop can not be computed from first principles. The pressure drop is calculated based on the Darcy-Weisbach

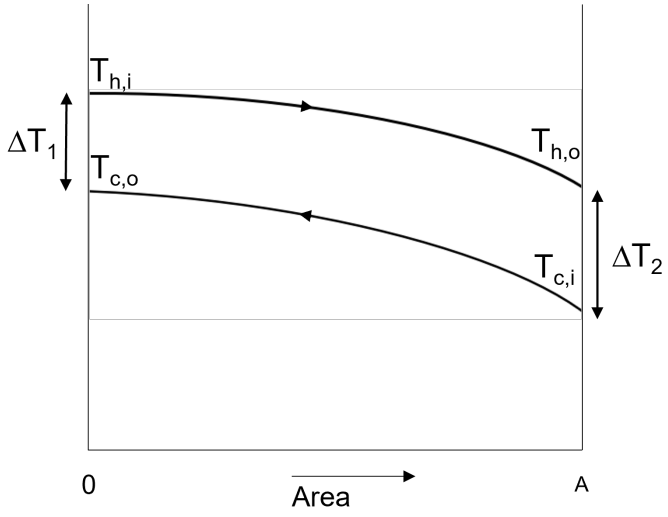

FIGURE 2.4: Temperature distribution in a counter-current flow arrangement

equation 2.8 (Brown, 2003). The pressure drop is proportional to the square of the flow velocity. Other factors are the hydraulic diameter of the pipe, D_{H}, the density of the fluid, ρ, L is the length of the pipe and f_{D} is the Darcy friction factor (Brown, 2003). The latter has to be solved experimentally due to the complex nature of GPHEs. The hydraulic diameter provides an approximation of the flow behaviour.

$$\Delta p = f_{\mathrm{D}}\ L\ \frac{\rho}{2}\ \frac{u^2}{D_{\mathrm{H}}} \tag{2.8}$$

The pressure drop characteristics vary with the type and configuration of GPHE. In this section the characteristics are based on a counter-current GPHE with single-phase fluids. The pressure begins to drop at the inlet connection since the hole in the cover plate has a diameter smaller than the pipes. After the connection, the pressure

generally increases (Sundén and Manglik, 2007). Two factors influence the change in pressure in the port. As the media flows past the plates, there is friction between the media and the plates. The friction decreases the pressure. As the media flows through the port, some of it goes straight forward and some of it passes though the channels. We therefore have a reduction in volume flow rate the further down we go into the port. This affects the pressure through Bernoulli's principle which states that the relationship between pressure and flow rate is inverse for an ideal, frictionless and incompressible fluid that flows horizontally (Qin and Duan, 2017). Since the pipe diameter does not change in the port, the volume flow rate is proportional to the flow velocity. Thus, as the media flows down the port, the flow rate decreases and the pressure increases as seen in Bernoulli's constant equation 2.9 (Qin and Duan, 2017).

$$\frac{v^2}{2} + gz + \frac{p}{\rho} = constant \tag{2.9}$$

The pressure increase is generally larger than the loss caused by friction, therefore the overall pressure is generally increased as the media flows down the port (Sundén and Manglik, 2007). The port on the other side of the channels, the outlet side, behaves differently in terms of pressure. Since media flows out from the channels here, the volume flow rate increases closer to the port and not the other way around. Since the effect from friction is the same the effect from both friction and the change in volume flow rate is a gradual and monotonic decrease in pressure through the port towards the connection.

Turbulence is good for the performance of the heat exchanger since it means that media is getting mixed around, allowing for a higher heat transfer rate. The cost of turbulence is an increased pressure drop. The only pressure drop that is not sought after, in the channels, is pressure drop at the adiabatic zones since there is no liquid on the other sides of these and therefore there is, almost, no heat transfer occurring at that position. At the other end of the plates, in the outlet port, the pressure drops with the distance to the outlet connection and within the connection as well.

The pressure drop of the GPHE can be customized. Usually, when a GPHE is bought, it has restrictions on the pressure drop, for example max 100kPa. Thus, when deciding on which GPHE to sell to the client the pressure drop must be considered, usually the pressure drop is maxed out. That is, the pressure drop is fully used and the delivered heat transfer area (length and number of plates) can be minimized to be able to offer a good price to the customer. To fully utilize the pressure drop, the GPHE can be designed and configured with great customizability, such as the pattern of the plates, the length of the plates and the pattern depth.

2.1.4 Fouling

Fouling can be defined as "the accumulation of undesired deposits on the heat transfer surface" (Sundén and Manglik, 2007, p. 181) and it comes in many forms. For example algae, minerals, calcium and silicates. As these materials are deposited in the heat exchanger the flow area is narrowed which leads to an increase in flow velocity for a constant volumetric flow rate and consequently an increase in pressure drop (Sundén and Manglik, 2007). As a result, the heat transfer coefficient can increase due to convection since the flow is more turbulent. However, the end result of the foulant deposit is a decrease in the overall heat transfer rate. This behavior can be seen in equation 2.6. The fouling resistance is correlated with the inverse of the overall heat transfer coefficient U.

Fouling occurs most frequently in areas where the shear stress is lower, since the flow in GPHEs is not symmetrical some areas experience lower shear stress than others and these are more susceptible for fouling. Thus, fouling can also cause maldistribution within the GPHE which also leads to a decrease in efficiency (heat-transfer per unit pressure drop).

Given that most heat exchangers will experience fouling sooner or later, it has to be included in the design process. When a customer orders a heat exchanger, it must be taken into account that the efficiency will go down, to sustain the same heat transfer as before the

pressure drop will have to increase. Therefore, GPHEs are usually designed with a heat transfer area margin that allows for some fouling. The heat transfer area margin effectively means that there is a margin for an increase in the pressure drop to compensate for the decreased efficiency.

2.2 Data analysis

During this thesis, data will be collected with the purpose of finding a way of measuring the flow in a GPHE and evaluating two sensor kits. To this end, it is important to go through the different techniques and principles that can be used for data analysis. The section begins with a discussion regarding the choice of statistical methods.

When building a prediction model, the goal after data gathering is to estimate the function f that describes the relation between the independents X and the response Y (James et al., 2021). When choosing how to estimate f, the purpose has to be taken into consideration. In *An introduction to statistical learning* by G.James et al (James et al., 2021) the why can be divided into two reasons: *prediction* and *inference*. When the goal is to simply predict the respondent and less care is spent on the details of the relationship between X and Y, the reason is said to be *prediction*. Other times, the specifics might be of interest. For example, the question could be if the relationship between X and Y is linear or non-linear, or in the case of multiple regression, which predictor has the most influence and the characteristics of that influence. In those cases, the reason is *inference*. Not all cases can be put into one category, sometimes the reasons overlap and both *prediction* and *inference* are of interest. The reason for estimation should be used to guide the choice of statistical method. For example, many advanced machine learning methods function as black boxes giving limited information about the characteristics of the function f, such methods should not be used when *inference* is the main goal.

G.James et al (James et al., 2021) argue that it is better to always try simpler methods when deciding on a model. Because, if they work they are likely to be more reliable and easier to fit and comprehend (James et al., 2021). This goes well with *Occam's razor* principle:

when faced with several methods that give a roughly equivalent performance, pick the simplest (James et al., 2021).

2.2.1 Data cleaning and preparation

Some machine learning methods are sensitive to the scale of the predictors. Large variables will have a larger effect on the outcome than small variables. To illustrate, imagine a model that has the temperature and the energy demand per day in Scania as independents. The temperature is in Celsius and the energy demand is in MWh. The difference in scale between 20C and 35000MWh can cause issues in certain models such as K-nearest neighbours (James et al., 2021). To overcome these issues the predictors can be *standardized*, and the predictors are given a mean of zero and a standard deviation of one (James et al., 2021). For some models, re-scaling each variable to fit between 0 and 1 is more suitable, this technique is called *normalization* (Lee, 2019).

Data is often gathered through experimentation. During experimentation errors occur frequently, due to sensor faults, electronic mishaps and more. The errors can produce *outliers*, data points that lie outside the rest of the data (Lee, 2019). These outliers can have a large effect on the performance of machine learning models and it is important to keep track of outliers when analysing data. They might need to be removed. In the book *Python Machine Learning* by Wei-Meng Lee two techniques that can deal with outliers are presented: Tukey fences and Z-score. Tukey fences are based on the quartiles of the data while Z-score uses standard deviations (Lee, 2019). Since the techniques have different methodologies they also give different results, there is no best technique, it has to be decided on a case-by-case basis.

2.2.2 Linear regression

One of the most commonly used statistical tools, both simple and intuitive, is linear regression. The word linear comes from the relationship between the response Y and the regression parameters. Multiple linear regression is shown in equation 2.10, the parameters are

β_0, β_1 and β_2, and the name *linear* stems from the linear relationship between the parameters and the response.

$$Y = \beta_0 + \beta_1 X_0 + \beta_2 X_1 \tag{2.10}$$

Linear regression is the estimation of these parameters to achieve as good a fit as possible. A measure of the goodness of the fit is required, the most common one is least squares (James et al., 2021). A metric called residual sum of squares RSS is calculated by adding up the squared residuals (James et al., 2021). The fitting process is the process of minimizing RSS, hence the name *least* squares (James et al., 2021). Sometimes there are multiple predictors and we can find ourselves in a position where we want to predict the response using all of these predictors. If we do a separate regression for all of the predictors we might run into issues. For instance, if we want to predict the weight of a child we might use height and age as predictors. If we do separate regressions the estimated effect might be substantially larger than the true effect, this is because the predictors are correlated (James et al., 2021). A taller child is more likely to be older but the model does not take this into account. Therefore, to get a better estimate, both predictors should be used in a multiple linear regression as shown in equation 2.10.

Sometimes when dealing with data, you can end up with two predictors that work in synergy. The effect on the response from a change in both predictors is larger than an equally large change for only one of the predictors (James et al., 2021). To circumvent this issue an interaction term can be added. The interaction term is the product of the two predictors. Multiple linear regression with interaction term is shown in equation 2.11. When using an interaction term, the involved predictors should always be included according to the *hierarchical principle* (James et al., 2021). By leaving them out, the characteristics of the interaction term can change.

$$Y = \beta_0 + \beta_1 X_0 + \beta_2 X_1 + \beta_3 X_0 X_1 \tag{2.11}$$

The model is extended by introducing ways to work with non-linear behaviour. In some cases the relationship between the predictor and the response is not linear, if we want to continue using linear regression we have to transform the data to get a good fit. Since the word linear only relates to the parameters, the data points themselves can be transformed by taking the square, the cube et cetera. This extension is called polynomial regression (James et al., 2021).

2.2.3 Evaluating sensor accuracy

Four metrics very used to evaluate the sensor accuracy, mean absolute error (MAE), root mean square error (RMSE), mean percentage error (MPE) and mean absolute percentage error (MAPE).

$$\text{MAE} = \frac{1}{n}\sum_{t=1}^{n}|Y_t - \hat{Y}_t| \tag{2.12}$$

The mean absolute error is calculated by taking the mean of the absolute value of the residuals, as seen in equation 2.12 (Willmott and Matsuura, 2005). The RMSE, shown in equation 2.13, is a similar metric but it has some significant differences that are important to be aware of (Willmott and Matsuura, 2005). Most importantly, the RMSE scales with the size of the measurement with a lower limit of MAE and an upper limit of $\text{MAE} \cdot n^{1/2}$. Thus, the interpretation of RMSE is therefore ambiguous (Willmott and Matsuura, 2005). However, it still has its uses. As a result of taking the square of the error, greater errors have a proportionally larger influence (Willmott and Matsuura, 2005). Consequently, the difference between the MAE and RMSE can be used as an indication of greater variance in the sample.

$$\text{RMSE} = \sqrt{\frac{1}{n}\sum_{t=1}^{n}(Y_t - \hat{Y}_t)^2} \tag{2.13}$$

When interested in whether a model or sensor overestimates or underestimates, the metric MPE can be used for identifying under- and

overestimation. If the metric is close to zero neither is present. Otherwise, a positive number indicates underestimation and a negative number overestimation. The metric is shown in equation 2.14 (Hanke and Wichern, 2013).

$$\text{MPE} = \frac{1}{n}\sum_{t=1}^{n}\frac{(Y_t - \hat{Y}_t)}{Y_t} \tag{2.14}$$

The MAPE is also based on dividing the error with the reference value. However, compared to MPE, MAPE takes the absolute value of both the error and the reference value (Hanke and Wichern, 2013), see equation 2.15. By doing so, before taking the mean of the calculated quotient, the quotients are not cancelled out by each other as they are with MPE. Therefore, MAPE is especially useful when the relative size of the error is relevant.

$$\text{MAPE} = \frac{1}{n}\sum_{t=1}^{n}\frac{|Y_t - \hat{Y}_t|}{|Y_t|} \tag{2.15}$$

Chapter 3

Sensors

3.1 Flow switch

Measuring the flow of gases and liquids can be of great value in the process and manufacturing industry. Some devices measure the flow and respond only when the flow goes above or below a threshold. These devices are called flow switches. In contrast to flow meters, the purpose of a flow switch is not to get a continuous measurement of the flow. However, if they could they would be of great value since they are cheap and easy to install.

One type of flow switch is the calorimetric flow switch. The specific design of such a flow switch might vary. The description that follows explains how the flow switch used in this thesis functions.

The flow switch has a probe that is inserted into the pipe, optimally the tip of the probe is located at the area of maximum flow velocity which normally is in the centre of the pipe (insertion length equal to half the inner diameter of the pipe), see figure 3.1. The probe has a heating element and two temperature sensors, depicted in the figure in red and blue respectively. When media, such as water, flows by the probe tip the media will carry heat away. A higher flow means that more heat will be carried away. This can be detected either by measuring the difference in temperature at the tip and a bit above the tip or by measuring how much energy is required to keep the temperature difference between the two sensors constant. The temperature sensor located a bit above the tip should be located on the side of the tip

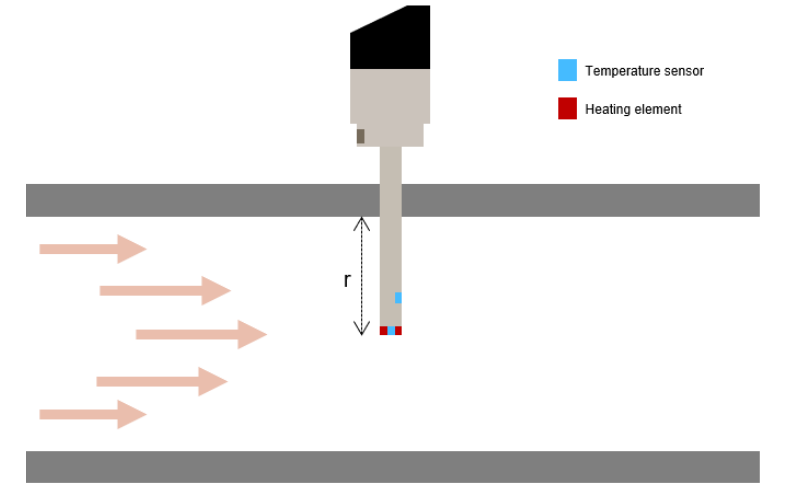

FIGURE 3.1: Calorimetric flow switch

facing away from the flow. Since the temperature sensor is embedded it can not be seen during installation, a guide mark is used instead. The guide mark should face the flow, it is shown in the figure as the small gray box facing the flow on the part of the sensor that protrudes from the pipe. According to the manufacturer, the accuracy of the flow switch decreases with an increase in the flow velocity and the temperature of the media. The flow switch is said to have a settling time of 5-10 seconds. That is, the time interval from a change in flow to the sensor measuring a steady state. The flow switch has a display where data such as the temperature and flow velocity can be seen. The flow switch has an analogue 4–20 mA output signal. The current corresponds to the flow velocity where 4 mA is 0 m/s and 20 mA is 3 m/s. To calibrate the sensor a multiplier called muF can be changed. The muF multiplier simply multiplies the sensor output to get the "true" value as seen in equation 3.1. It is also possible to set the current flow to zero.

$$muF = \frac{\text{True value}}{\text{Sensor output}} \tag{3.1}$$

3.2 Sticker sensor

The sticker sensor is a small device that can measure both strain and temperature. With these measurements it is possible to get the pressure by using machine learning models. Due to its small size, it can be put into positions where other sensors can not fit. One such position is the backmost plate in a GPHE. The sensor is highly advanced and uses nanoparticles to measure the strain. The sticker sensor is made by printing nanoparticles in a specific pattern. As the sensor is strained the pattern changes shape which results in a change in electrical resistivity. Since the resistivity also depends on the temperature, the temperature has to be measured as well. In an IoT application, a long battery life is valuable. Poor battery life can be a nuisance for customers who have to change the battery themselves or contact the provider to come to change it. For the supplier, any nuisance for the customer is bad news. Even if the supplier keeps track of the battery life and changes it on its own, the customer still has to prepare for such a visitor, by for example moving heavy machinery in the way of the sensor or temporarily shutting down operations.

The sticker sensor described here has a very good battery life because it uses a high resistance, and thus low current. The sticker sensor has been tested with GPHEs before, during these tests the sticker sensors performed quite well but they showed reduced pressure accuracy when exposed to a fast change in temperature or pressure drop, the reason of which is unknown. One cause could be hysteresis, a behaviour where the sensor measurements are dependent on the previous states of the system. During this event, the flow on one side (side 1 or side 2) was kept constant while the other one was dropped from 30 l/s to 5 l/s. Thus, the change in flow on one side may have an effect on the accuracy of the other side.

3.3 In-house kit

The in-house kit uses the deformation of a diaphragm to measure the pressure. The diaphragm is located in a cavity of the sensor. The in-house kit also measures the temperature. Previous experiments have shown that the surroundings affect the temperature measurements.

The temperature sensor was heated and cooled not only by the media but also by the surrounding material and ambient air. To limit the heat transfer to the ambient air, insulation material was put on the sensors. A compensation model was set set up to compensate for the effect of the surrounding material on previous installations. The model depends on the type of material, the thickness and the surface area between the device and the material. Since the installation in this thesis is novel, the model will have to be adjusted. In addition to the surrounding material, the ambient temperature can also cool or heat the device either directly or through the surrounding material. This could cause measurement errors and might have to be included in the model.

Chapter 4

Methods

This chapter presents the methodology employed to improve Alfa Laval's service capability by testing inexpensive sensors. In this thesis, the primary objective was to evaluate the accuracy of a flow switch in measuring the flow in a GPHE. The secondary objective was to assess the reliability and accuracy from two other sensor kits, an in-house kit and a sticker sensor kit. The selected methodology incorporates a combination of test design, data collection, and modeling techniques to analyze the accuracy and reliability of various sensor solutions.

Laboratory experiments were conducted at Alfa Laval to assess the performance of the sensors in a realistic scenario. The collected data were analyzed, visualized, and subjected to statistical analysis to derive insights and evaluate the suitability of the sensors. Additionally, some of the data were utilized to create models aimed at enhancing the accuracy of the sensors.

4.1 Lab setup

Alfa Laval has a lab with sophisticated equipment for testing products, among them GPHEs. During my thesis, two thermal rigs were used, both positioned in the lab. These rigs are designed for evaluating the performance of heat exchangers and to investigate the HE characteristics. An external heat exchanger can be connected to the thermal rig. The connected GPHE can be run with the thermal rig

controlling the flow rate, temperature and pressure drop. A simplified description of the thermal rigs process control is as follows: The flow rate is controlled by pumps and control valves while the temperature is controlled by using two GPHEs and control valves. The flow rate can be changed rapidly, it only takes a couple of seconds while changes in temperature take a lot more time, up to 10-15 minutes.

The two thermal rigs are of different sizes, one small, and one large. The large one is capable of handling higher volume flow rates than the small one. They can handle about 60 liters/s and 12 liters/s respectively. A GPHE, of the type M10, was available, it was connected to both thermal rigs, first the small then the large. The M10 GPHE was configured with a small plate package (only a few plates) when connected to the small thermal rig which was expanded to a large plate package (a couple of dozen plates) before it was connected to the large thermal rig.

Seven test sessions were run. For the first four test sessions, a small plate package was used. Later, the large thermal rig was used to enable even higher flow velocities. The plate package had to be increased when moving the M10 to a large thermal rig since the pressure drop would reach too high levels otherwise.

Sensors were installed on the connected GPHE i.e. the M10, both GPHEs in the small thermal rig and one GPHE in the large thermal rig. An overview is shown in table 4.1. It shows which sensors where used during each session and the sampling time of the sensor. For example, during session one, the M10 had two sets of sticker sensors and one in-house kit installed. The T8s (part of the small thermal rig) had two in-house sensor kits installed.

TABLE 4.1: Overview of sensor setup

Session/Sensor	Sampling time	Thermal rig	GPHE
Session 1			
Sticker sensor 4×2	1 s	Small	M10
In-house 4×3	10 min	Small	T8×2 & M10
Sessions 2–4			
Sticker sensor 4×2	1 s	Small	M10
In-house 4×3	10 min	Small	T8×2 & M10
Flow switch × 2	1 s	Small	T8×2
Sessions 5–7			
Sticker sensor 4×2	1 s	Large	M10
In-house 4×2	2 s	Large	M10 & M15
Flow switch	1 s	Large	M10

4.1.1 Tests with the small thermal rig

The small thermal rig uses two T8 GPHEs to control the temperature. The T8s control the inlet temperature for each side of the connected heat exchanger, which in this thesis is an M10. Both the T8s and the M10 used a counter-current flow arrangement. A photo of the small thermal rig with the M10 connected is displayed in figure 4.1.

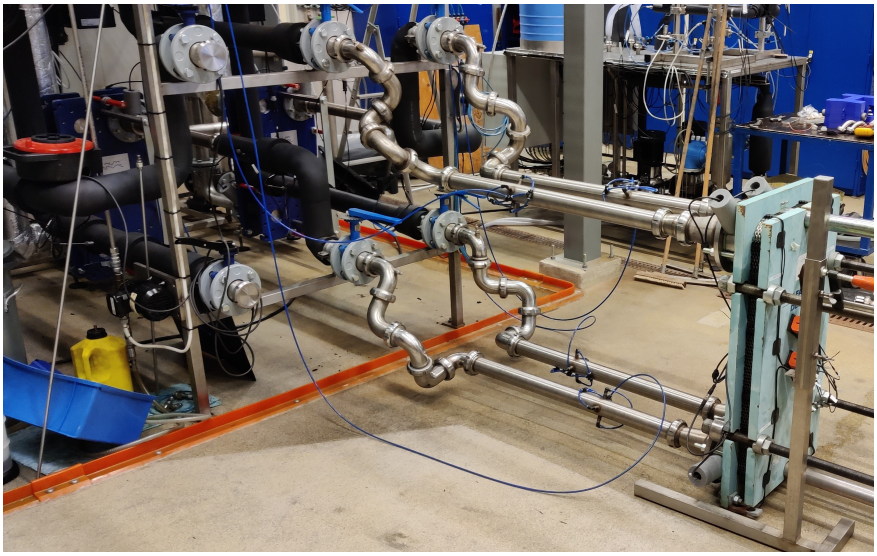

FIGURE 4.1: The small thermal rig with the connected M10 GPHE

The sensor kits were complemented with the sensors permanently installed on the thermal rigs, temperature sensors, pressure sensors and magnetic flow meters. All with a sampling rate of 1 Hz. The sensors are calibrated once every year. The thermal rig uses two temperature sensors for each port. The temperature sensors are mounted on pipes connecting the thermal rig to the GPHE, see figure 4.2.

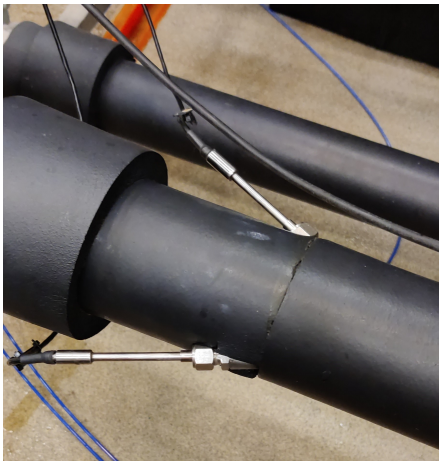

FIGURE 4.2: Temperature sensor on the small thermal rig

The heat exchangers do not come with a slot where the in-house sensors can be installed, the solution was a connector, a metal flange with an inner diameter slightly larger (T8: 89 mm, M10: 110 mm) than the pipe's inner diameter (T8: 80 mm, M10: 100 mm). Each connector has two threaded holes where an in-house sensor or flow meter can be fastened. Each T8 has one port with piping connecting the port directly to the M10, on this port it was not possible to mount a connector due to the size constraints of the thermal rig, therefore, a threaded cylinder was welded onto the pipe, viewed in figure 4.3b. Since the sensor needs to be in contact with the medium, a hole was drilled through the pipe before welding on the cylinder.

Four in-house sensors were installed on each T8, one for every inlet and outlet. After the first session, one flow switch was installed on each T8. To be able to compare the measurements from the flow switches to the thermal rigs the flow switch had to be mounted on the same side i.e. the side where the media flows through the T8 to the M10. The flow switch can be seen in the lower left of figure 4.3a, it is the device with a red display.

The flow switch measures the flow velocity (m/s). By entering the pipe diameter the sensor output can be changed to the volume flow rate. Since the flow switches were mounted on connectors with an inner diameter of 89mm (T8s) and 110 mm (M10s) these were added to the sensor settings. Note that the inner diameter of the connectors is larger than the inner diameter of the pipes (80mm for T8s, and 110mm for M10s).

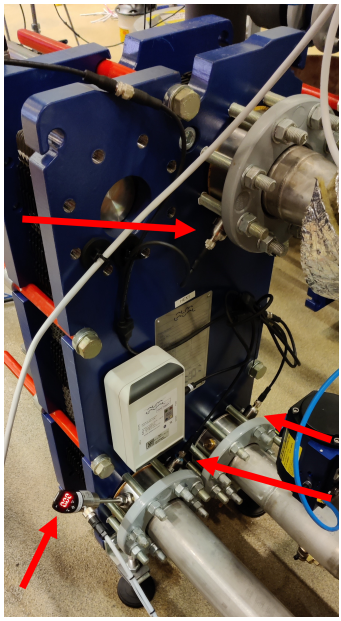

(A) T8 with in-house sensors and flow switch installed

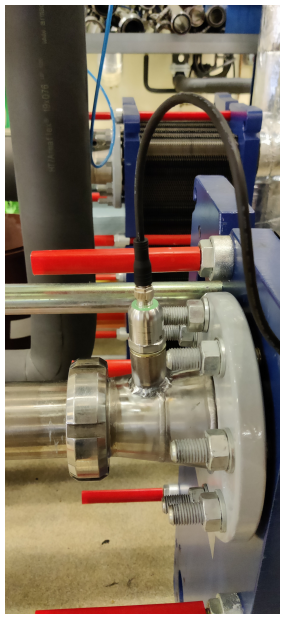

(B) Welded cylinder with threaded hole for in-house sensor

FIGURE 4.3: Sensors installed on the T8 on side 2 (cold side)

During the test sessions performed with the small thermal rig, the M10 GPHE had two sensor types connected: sticker sensors and in-house sensors. As mentioned in Chapter 3, the sticker sensors measured strain and temperature while the in-house sensors measured pressure and temperature.

The sticker sensors were mounted on the plate furthest back in the plate package. There was a risk of damaging the sticker sensors when pushing the plates together, therefore a metal plate cover was put on top of the back plate with cutouts for the sticker sensors.

4.1.2 Tests with the large thermal rig

The large thermal rig has two M15 HEs that control the temperature, instead of the T8s in the small thermal rig. One of these M15s was fitted with a set of four in-house sensors. The M15 also used a counter-current flow arrangement. The M10 was altered slightly when it was moved from the small thermal rig to the large thermal rig. The plate package was extended to 49 plates from 10, a flow switch was installed on the inlet of side 2 and the in-house sensor kit was updated to allow for a 1s sample time instead of 10 minutes. A picture of the M10 after the changes is shown in figure 4.4.

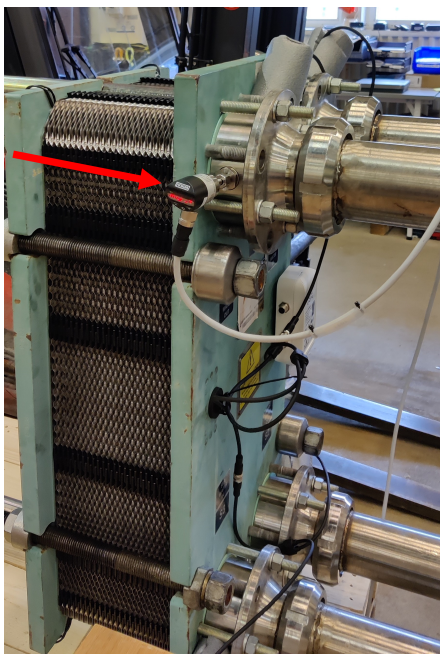

FIGURE 4.4: M10 connected to the large thermal rig

4.2 Test plan

Now that the tools used in the tests have been presented, it is time to describe how the tests were planned and carried out. The first test session was planned by the sticker sensor supplier as they wanted to generate data to calibrate their sensors. During the first session, the flow switches had not been installed yet. The test plan of the second session was designed based on the knowledge gathered from the sensor data sheets, previous papers and articles and from discussions with my supervisor and co-supervisor at Alfa Laval. Due to the difficulty of precisely controlling the test parameters i.e. temperature and volume flow rate, the test plan could not be followed with perfect accuracy. The test plan for the second session is shown in table 4.2.

TABLE 4.2: Test plan for session two. The volume flow rate was calculated based on the hydraulic inner diameter which is the ports and pipes inner diameter.

Temperature [°C]		**Volume flow rate [l/s]**		**Flow velocity [m/s]**
Side 1	Side 2	Side 1	Side 2	T8 connections
50	15	2	2	0.40
50	15	6	6	1.19
50	15	12	12	2.39
50	15	6	6	1.19
50	15	2	2	0.40
65	15	2	2	0.40
65	15	6	6	1.19
65	15	12	12	2.39
65	15	6	6	1.19
65	15	2	2	0.40
80	15	2	2	0.40
80	15	6	6	1.19
80	15	12	12	2.39
80	15	6	6	1.19
80	15	2	2	0.40
50	15	6	6	1.19
50	15	12	12	2.39
50	15	6	6	1.19
50	15	12	12	2.39
50	15	2	12	2.39
50	15	12	2	0.40
50	15	6	6	1.19

The test sessions following the first were designed based on the results from the previous sessions. For example, if an anomaly was detected, one could wish to recreate the environment to see if such an anomaly is recurrent. As described in Chapter 3, the sensors have many limits that need to be tested to be able to understand the potential of the sensors in terms of what they can handle. One potential issue that was noticed during previous testing was a possible hysteresis effect of the sticker sensors. To investigate this effect, a test had to be designed with temperature and pressure changes, in both directions. The other possible reason for the undesirable behaviour of the sticker

sensor, previously brought up in Chapter 3, was that the volumetric flow was kept constant on one side and changed on the other. To see if the sticker sensors were sensitive to such situations they were recreated, for example by keeping the volumetric flow rate constant at 12 l/s on one side and changing the other to 2 l/s.

Moving on to the flow switch, it uses the calorimetric principle in which two temperature sensors are positioned inside a probe that is inserted into the centre of the pipe. The flow switch sensitivity to temperature and flow velocity, when connected to a GPHE, is unknown. According to the manufacturer's datasheet, the accuracy is reduced with an increase in either temperature or flow velocity. Consequently, the tests were planned so that the accuracy of the flow switch could be tested with as large a range in temperature and flow velocity as possible.

Due to the limits of the small thermal rigs, the volumetric flow rate had to be kept within 2–12 l/s which corresponds to 0.4–2.39 m/s in the T8s ports (80 mm inner diameter). During the test sessions with the large thermal rig, the volume flow rate was mainly kept between 10–55 l/s which corresponds to a, partly overlapping, flow velocity range of 1.27–7.00 m/s in the M10 ports (100 mm inner diameter).

After the second session, a third session was planned based on the results of the two previous sessions, the fourth session on the three previous and so on. All sessions were not planned in advance. Since the data were monitored live, observed interesting behaviour sometimes led to the test parameters being decided on the go.

4.3 Data analysis

Three models were used to fit the volume flow rate measured by the flow switch to the true values (thermal rig). The data from side 2 of session four was used. The first model was a simple linear regression shown in equation 4.1. The second model included the temperature measured by the thermal rig which was assumed to be similar to the temperature at the flow switch, see equation 4.2. The third model

extended the second model by adding an interaction term, see equation 4.3. The estimated volume flow rate, volume flow rate measured by the flow switch and temperature are depicted by Q_{est}, Q_{fls} and T.

$$\text{Model 1: } Q_{est} = \beta_0 + \beta_1 Q_{fls} \tag{4.1}$$

$$\text{Model 2: } Q_{est} = \beta_0 + \beta_1 Q_{fls} + \beta_2 T \tag{4.2}$$

$$\text{Model 3: } Q_{est} = \beta_0 + \beta_1 Q_{fls} + \beta_2 T + \beta_3 Q_{fls} T \tag{4.3}$$

The data were fitted using the Python *statsmodels* library.

Chapter 5

Results

In this chapter, the experimental results are presented together with the results from the data analysis. The chapter begins with a presentation of the data from the thermal rig. Then, the results are presented for the sensors, with one section for each sensor.

5.1 Thermal rig

A time series of the volume flow rate and temperature are shown for every session to give you a good overview of the experiments. The sessions have been divided into two groups, sessions 2–4 and sessions 5–7. The groups represent test sessions with different thermal rigs, sessions 2–4 were with the small thermal rig and 5–7 with the large thermal rig.

5.1.1 Small thermal rig

The volume flow rate for sessions 2–4 is presented in figure 5.1. The dotted yellow lines separate the sessions from each other, with session two being the one furthest to the left, session three in the middle and session four to the right. The sessions are also highlighted by the yellow numbers in the figures. The same logic applies to all other figures with yellow separators and numbers. The x-axis "Sample" is a time-series. Note that the time series has intervals between the

sessions, i.e. within a session, the time difference between two consecutive samples is one second, that is not the case between samples from different sessions.

The volume flow rate was kept between 2 and 14 l/s during sessions 2–4, as seen in figure 5.1a and 5.1b.

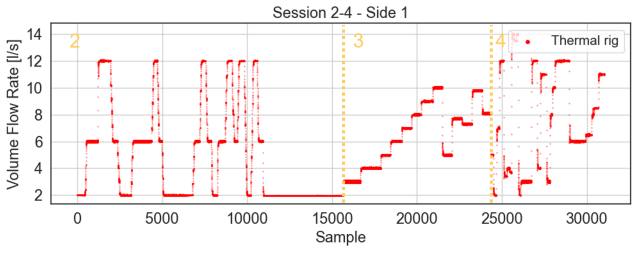

(A)

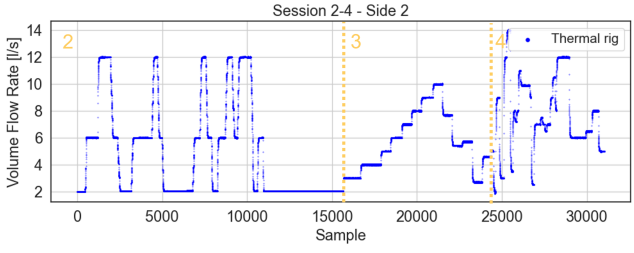

(B)

FIGURE 5.1: Shows the volume flow rate during sessions 2–4

The test plan of session two was presented earlier in table 4.2, the volume flow rate followed the plan almost perfectly. However, due to the limits of the thermal rig, the temperature could not keep up, see figure 5.2a and 5.2b. When changing the flow, it takes some time for the temperature to stabilize, consequently, the temperature could not be held at the levels given by the test plan.

During session three the volume flow rate was increased step-wise, from 2–10 l/s after which the volume flow rates were randomized to identify any unexpected behaviour. Throughout the tests, the volume flow rate was kept at certain steps, for example, 2, 6 and 12 litres, it is these steps that sometimes were randomized. The volume

flow rate was also randomized during session four, at each step the temperature was changed rapidly to investigate a temperature dependence observed in the flow switch, which is thoroughly investigated in section 5.2.

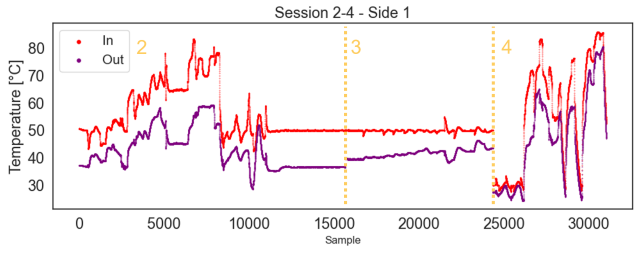

(A)

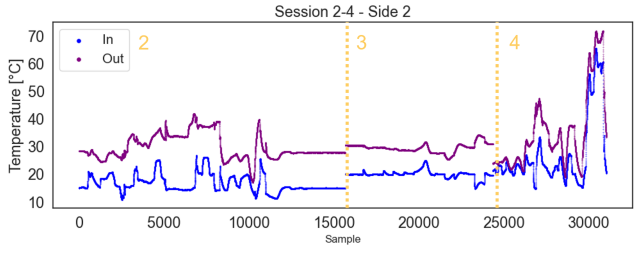

(B)

FIGURE 5.2: Shows the temperature during sessions 2–4. The temperature is measured between the M10s and the T8s

5.1.2 Large thermal rig

During sessions 5–7 the volume flow rate ranged between 10–55 l/s, see figure 5.3a and 5.3b. A test protocol similar to the one followed during session two was adhered to during session five. The difference was mainly the volume flow rate which was held at 10, 20 and 30 l/s instead of 2, 6 and 12 l/s. During session six and seven the focus was on high volume flow rates and the sensors performance over an extended period.

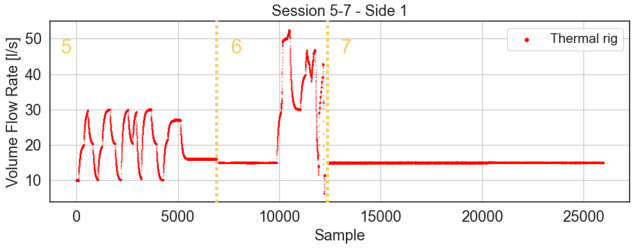

(A)

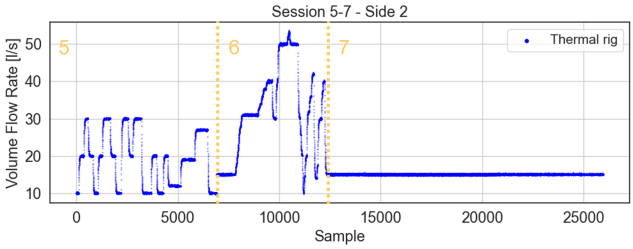

(B)

FIGURE 5.3: Shows the volume flow rate during sessions 5–7.

In contrast to the volume flow rate, the temperature was not strictly controlled during session five and six, see figure 5.4a and 5.4b. During session seven the temperature was kept constant for most of the time, with only one step change.

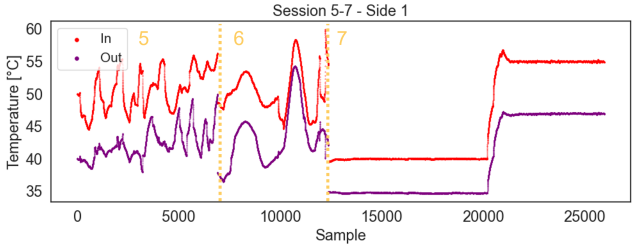

(A)

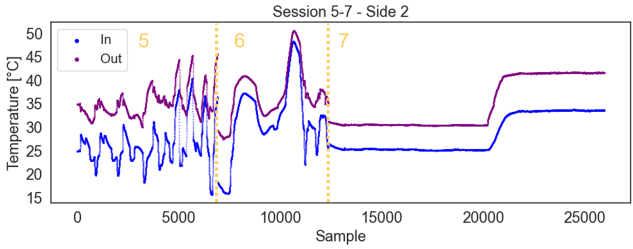

(B)

FIGURE 5.4: Shows the temperature measured by the thermal rig during sessions 5–7

5.2 Flow switch

In total, three flow switches were installed and tested. Two on the T8s during sessions 2–4 and one on the M10 during sessions 5–7. The volume flow rate measured by the thermal rig and flow switch is shown in figures 5.5a (Side 1) and 5.5b (Side 2). Note that the volume flow rate was calculated based on the hydraulic diameter i.e. the ports and the pipes inner diameter, not the connections.

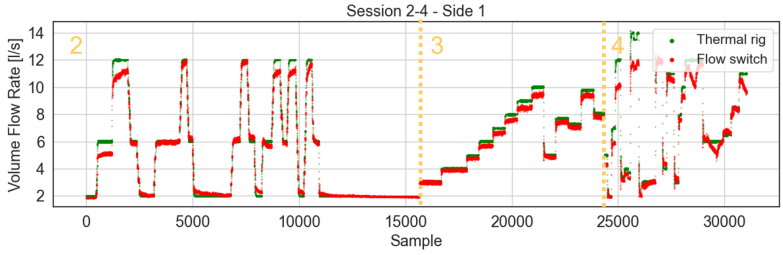

(A)

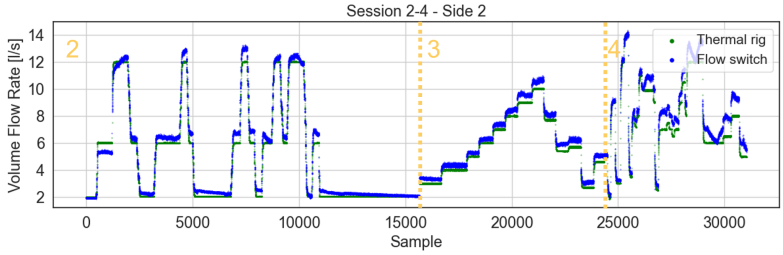

(B)

FIGURE 5.5: Shows the volume flow rate during sessions 2–4

Another comparison of the volume flow rate measured by the thermal rig and flow switch is shown in figure 5.6. The thermal rig is on the x-axis and the flow switch is on the y-axis. The data included in the figure are from sessions 2–4. A perfect result where the flow switch measured the correct value every time would be a line where $x = y$. The flow switch performs well overall. The flow switch overestimates the volume flow rate slightly on side 2 and underestimates the flow slightly on side 1. The relationship is linear on both sides, they can therefore be calibrated using simple linear regression.

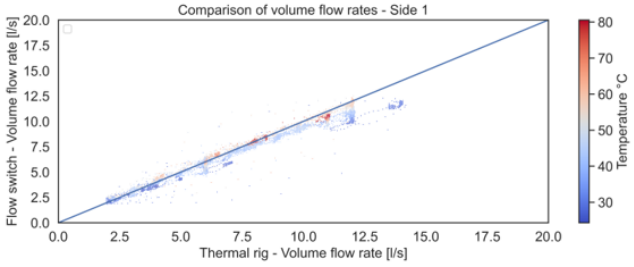

(A)

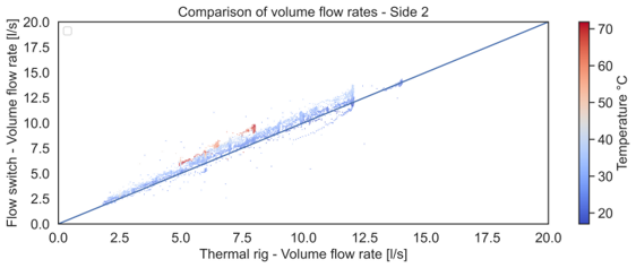

(B)

FIGURE 5.6: Highlights the difference in the volume flow rate measured by the thermal rig and the flow switch during sessions 2–4. The color represents the temperature at the time of measurement. Note the impact of the temperature, at a fixed true volume flow rate the value measured by the flow switch varies with the temperature, with a high temperature generally giving a higher measured value than lower temperatures

After analyzing the results from session two, an interesting behaviour was noticed, the output from the flow switch seemed to be correlated to the temperature. When the temperature increased, so did the volume flow rate measured by the flow switch. In figure 5.7a, the volume flow rate measured by the thermal rig is shown in colour and the thermal rig is shown in black. A darker red means that the temperature was high at that time, and a darker blue means that the temperature was low. To read the specific temperature the scale on the right can be used. The temperature dependence is most apparent when observing the peaks i.e. when the true volume flow rate is 12 l/s. The flow switch gives a higher reading when the temperature is

high (such as the peak before 10:30 and after 11:00), than low (9:30 and the two peaks between 11:30 and 12). This behaviour can also been when observing figure 5.6. Measurements at high temperatures are generally further away from the $x = y$ line than others.

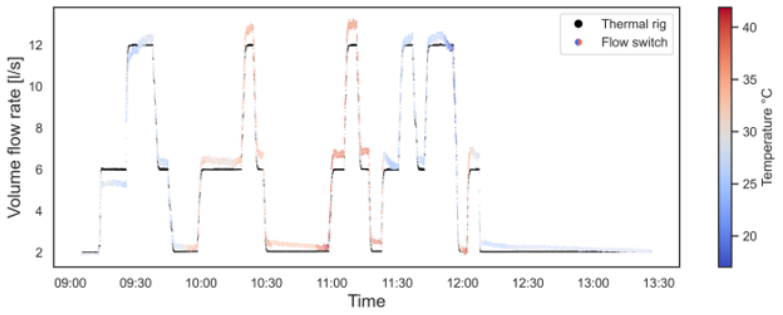

(A) Session two

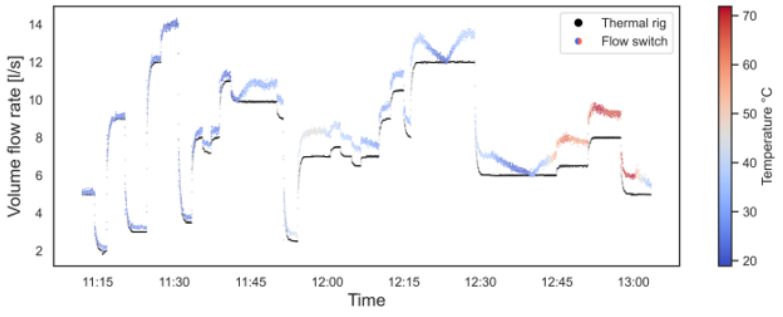

(B) Session four

FIGURE 5.7: Shows the volume flow rate measured by the thermal rig in black and the flow switch in color. The color of the flow switch curve indicates the temperature. Low temperature and high temperature are shown in dark blue and dark red, respectively, as shown in the temperature scale to the right

The temperature dependence was further analyzed in session four. The volume flow rate was kept constant while the temperature was changed, see figure 5.7b. The behaviour was most apparent at the second half of session four, from 11:45 and on wards. Between 12:15 and 12:30 the volume flow rate is kept constant at about 12 l/s while

the temperature is changed from $\sim$ 40°C to $\sim$ 25°C and up again. This variation in temperature correlated with a change in output from the flow switch from 14 l/s to 12 l/s and up to 14 l/s again. That is a decrease of 14%. The phenomena can also be observed in figure 5.6. A temperature gradient can be seen on the y-axis with darker red towards the top and darker blues towards the bottom of the measured flow switch values.

The flow switch performance during sessions 5–7 can be seen in figure 5.8. The true volume flow rate was kept between 10 l/s and 55 l/s (calculated using the hydraulic diameter) which corresponds to a flow velocity of 1.27 m/s and 7 m/s respectively, in the flow switch position. The limit of the flow switch as given by the manufacturer, 3 m/s, is therefore reached when the (true) volume flow rate is 23 l/s.

However, during the test session, the flow switch reached its limit at 33 l/s (4.20 m/s). Well above the limit as specified by the manufacturer. As the flow switch reached its limit it threw an error "0L" for too high flow velocity and gave a flat signal. Once the true volume flow rate reached an "acceptable" level again the error message disappeared and the sensor resumed normal operation.

During session six, an interesting behaviour was observed, just after the session started the reading from the flow switch suddenly dropped from 15 l/s to approximately 7 l/s. No parameter was changed, and the behaviour was completely unexpected. When the true volume flow rate was increased the flow switch seemed to follow the curve, but it dropped suddenly two more times. These two times, the drops were only temporary.

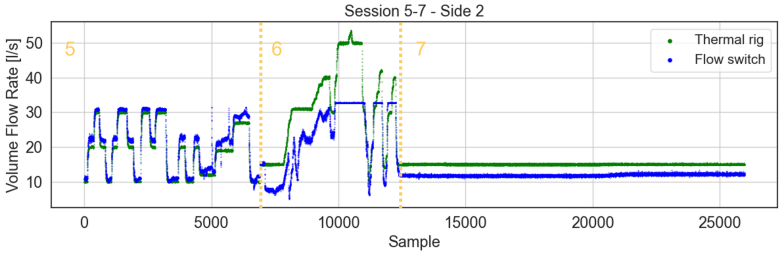

FIGURE 5.8: Shows the volume flow rate during sessions 5–7. The flow switch gave an error due to too high flow velocity, just before sample 10000, thus the flat line

Session seven is seen in the right most part of figure 5.8. The flow switch underestimates the volume flow rate consistently. There is a slight increase in the volume flow rate after sample 20000, which occurs simultaneously to an increase in temperature, shown previously in figure 5.4b.

5.2.1 Calibration and temperature compensation

To compensate for the temperature dependency of the flow switch three models were set up. The purpose of model 1 was to serve as a baseline for the others. It is a simple linear regression with the flow as an independent. Model 2 includes the temperature as well. Model 3 is an extension of the second, it adds an interaction term to account for the observation that the temperature dependency is higher at high flow rates than at low. The models were trained and tested on the raw data seen in 5.7b. The model coefficients are shown in table 5.1.

Model 1 adds a negative constant and scales down the volume flow rate with 4 %. Model 2 has a similar scaling coefficient but it also has a negative temperature coefficient. For every degree over 0°C the model compensates for the increase in the output from the flow switch by decreasing the estimated volume flow rate with -0.0254 l/s. For example, if the temperature is 50°C and the volume flow rate measured by the flow switch is 10 l/s, the estimated volume flow rate

will be 8.84 l/s $= 0.5534 + 0.9553 \cdot 10$ l/s $+ (-0.0254) \cdot 50°$C. In model 3 an interaction term was added to investigate the correlation between the volume flow rate (flow switch) and the temperature. The interaction coefficient is negative which means that the flow switch overestimates the volume flow rate more at higher temperature, which the negative interaction coefficient compensates for.

TABLE 5.1: The coefficients for models 1–3.

Independent	Model 1	Model 2	Model 3
Constant	-0.4153	0.5534	-0.5584
Volume flow rate - Flow switch	0.9633	0.9553	1.0920
Temperature - Thermal rig	x	-0.0254	0.0119
Interaction term	x	x	-0.0046

The first model, a simple linear regression, is shown in figure 5.9a where Q_{est} is plotted against the true volume flow rate. The fit is relatively good, certainly an improvement over the raw data. The fit of model 2 is shown in figure 5.9b. Notice the shape of the curve at the step after index 4000, it has shrunk somewhat. The fit is also improved for the steps before and after index 6000. Moving on to model 3, which extends model 2 by including an interaction term, the fit becomes even better judging by the naked eye, see figure 5.9c. For example, the fitted curve now fits the step after index 4000 very well, and the error seen in the step positioned in the middle of index 2000 and 3000 was almost completely removed.

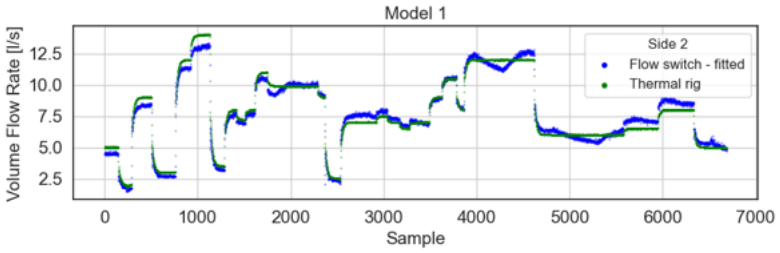

(A) Model 1

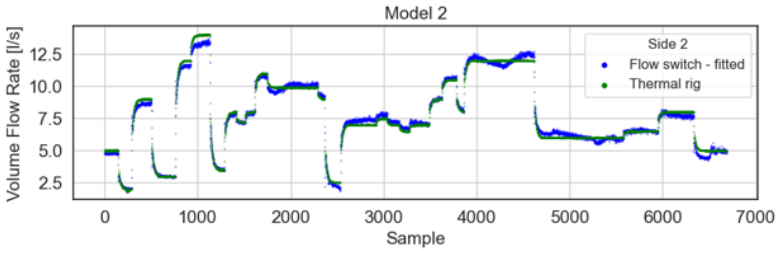

(B) Model 2

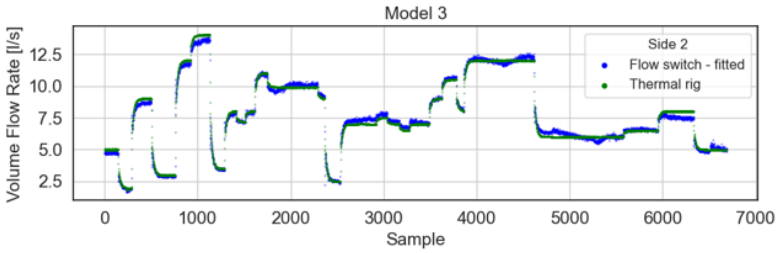

(C) Model 3

FIGURE 5.9: A visual depiction of the estimated and true volume flow rate for three different regression models

To get a thorough understanding of the performance of the models, the fitted values are plotted against the true values in figure 5.10. A line is plotted that corresponds to a perfect fit where $fitted\ value = true\ value$. Model 1 has a relatively good fit where the values are centred around the optimal line, however, few values are on the line itself. The next model, model 2 has a much more narrow distribution around the line which is further improved by model 3. Though

the difference between model 1 and two seem to be larger than the improvement from model 2 to 3.

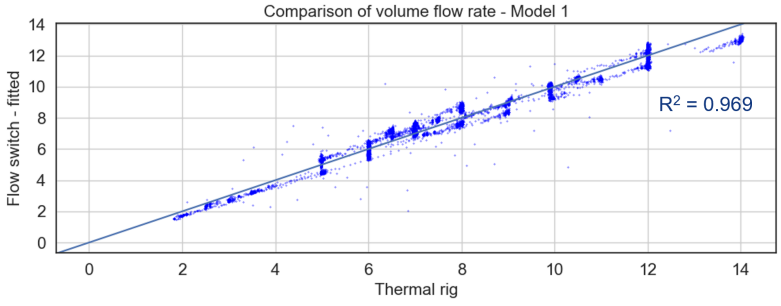

(A) Model 1

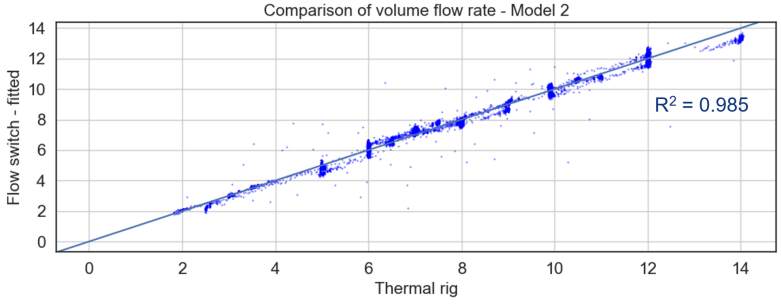

(B) Model 2

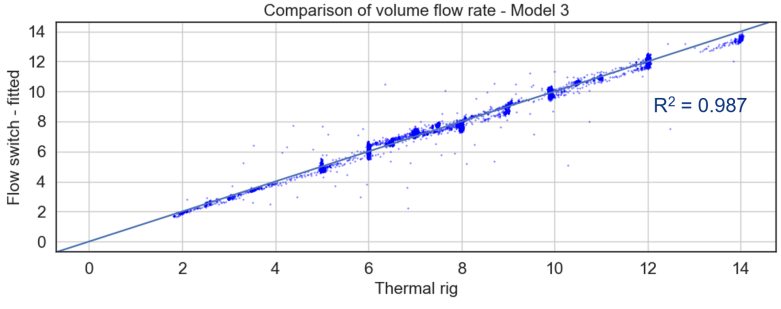

(C) Model 3

FIGURE 5.10: A comparison between the estimated and true volume flow rate for three different regression models

To complement the visual presentation, table 5.2 shows four metrics

for each model. The MAE is the highest with model 1 (0.40 l/s), decreases with model 2 (0.24 l/s) and even more with model 3 (0.22 l/s). The RMSE and MAPE follow the same trend. The metrics confirm what could be seen by the naked eye, that the models reduce the measurement error.

TABLE 5.2: Metrics describing the fit of the flow switch regression models

	MAE (l/s)	RMSE (l/s)	MAPE (%)
Model 1	0.40	0.49	5.69
Model 2	0.24	0.34	3.31
Model 3	0.22	0.32	3.11

5.3 Sticker sensor kit

The sticker sensor data were uploaded to, and processed by, the sensor supplier who then sent it to us. However, due to difficulties with the pressure calibration the supplier only sent temperature data. The data for session five and session six is presented in figures 5.11 and 5.12 respectively. During both sessions, the sticker sensors underestimate the temperature, the only exception that can be seen by looking at the graphs is "Side 2 - In" during session five, seen in figure 5.11c. The greatest difference between the estimated temperature and the true temperature can be seen by the naked eye in figures 5.11a and 5.12a representing "Side 1 - In" during session five and six respectively. However, since the scaling of the pictures differs, the statistics calculated in table 5.3 give a better understanding of the difference between the measurements.

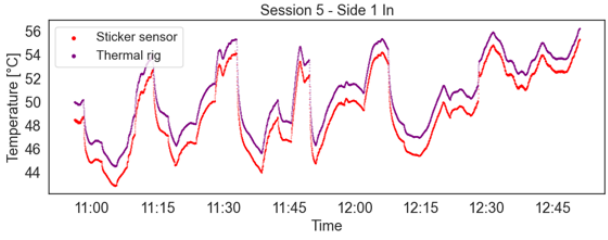

(A)

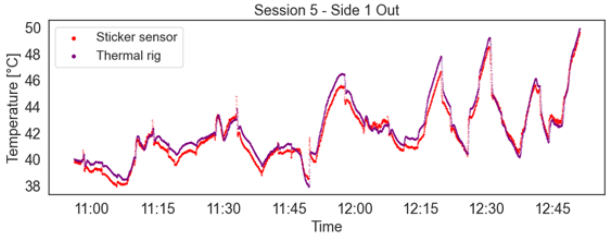

(B)

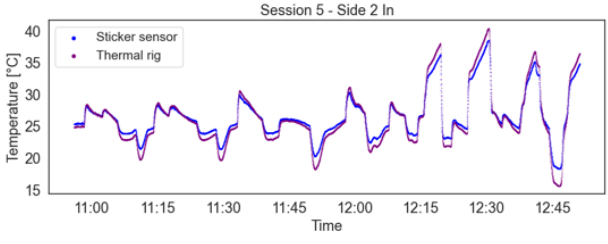

(C)

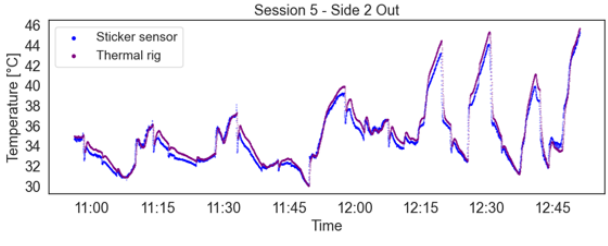

(D)

FIGURE 5.11: Shows the temperature data collected from the sticker sensors and thermal rig during session five.

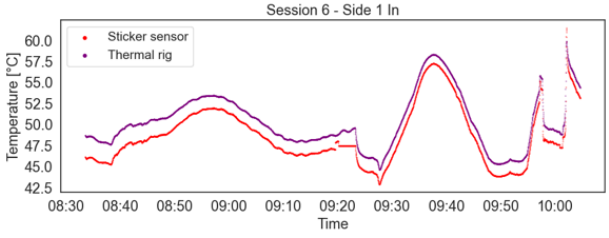

(A)

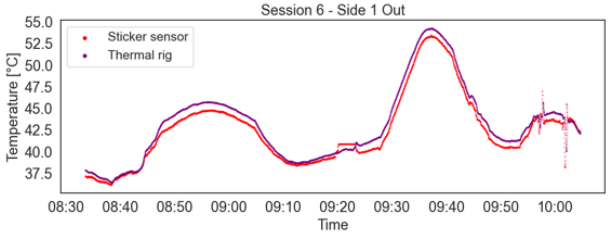

(B)

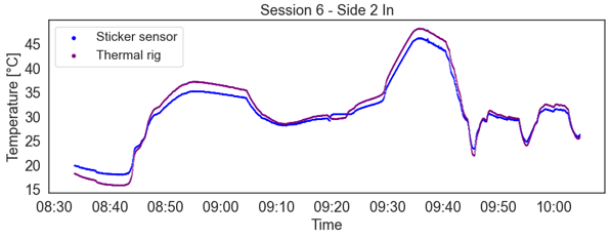

(C)

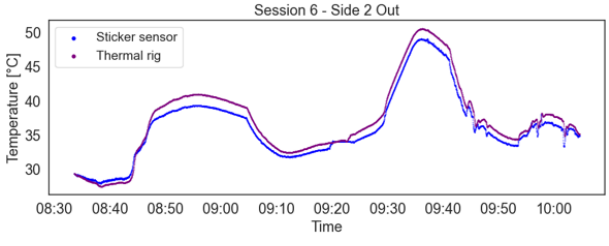

(D)

FIGURE 5.12: Shows the temperature data collected from the sticker sensors and thermal rig during session six.

Statistical measurements of the estimation error for the sticker sensors are shown in table 5.3. The mean absolute error ranges from 0.48 to 1.63, the RMSE has a slightly higher range of 0.58 to 1.67. Since the RMSE is more sensitive to variance than MAE, the difference between the RMSE and MAE can be used to indicate the spread of the data. In this case, the difference is very small indicating that the variance in the data is low. The MPE is positive for all ports and sessions except, "Side 2 - In" during session six. A positive MPE indicates an underestimation of the temperature, thus that is the general behaviour of the sticker sensors.

TABLE 5.3: Shows metrics for the temperature measurements by the sticker sensors. There are two values in each cell, the value to the left is from session five the other session six.

Port	MAE (K)	RMSE (K)	MPE (%)
Side 1 - In	1.43 / 1.63	1.44 / 1.67	2.86 / 3.27
Side 1 - Out	0.48 / 0.76	0.58 / 0.87	0.73 / 1.5
Side 2 - In	0.77 / 1.23	0.96 / 1.4	-1.66 / 0.76
Side 2 - Out	0.55 / 1.06	0.78 / 1.18	0.99 / 2.35

5.4 In-house kit

The data presented in this section are solely from sessions 5–7. During the previous sessions the in-house kits were configured to only save data once every 10 minutes, this was changed before session five to one sample every two seconds, dramatically increasing the amount of data collected. The in-house kit measures the temperature, see figure 5.13, and the pressure at each connection. The pressure can the be used to calculate the pressure drop after compensating for the hydrostatic pressure difference.

The pressure drop is shown in figure 5.14. After examining the temperature graphs it becomes apparent that the temperature measurements from the in-house kit are lagged i.e. they are shifted to the right relative to the temperature measured by the thermal rig. This

phenomenon becomes especially clear when observing the peaks of the temperature curves.

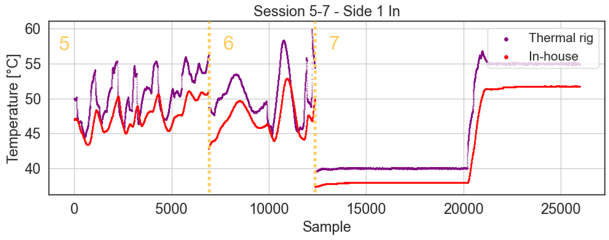

(A)

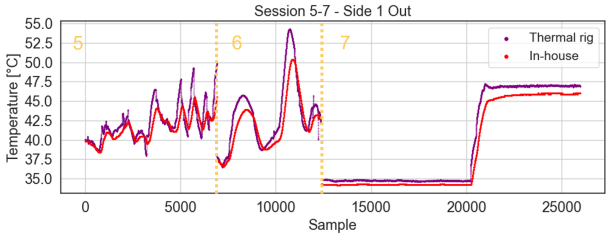

(B)

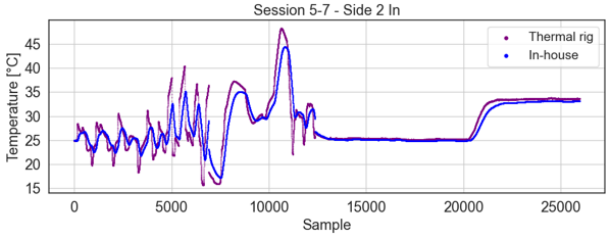

(C)

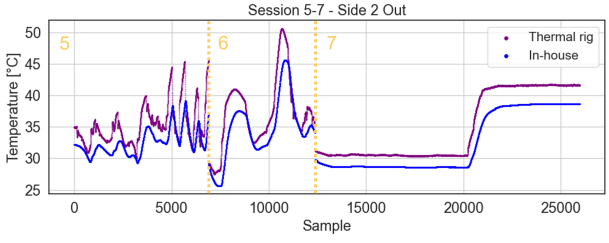

(D)

FIGURE 5.13: Shows the temperature data collected from the in-house kit and thermal rig during sessions five to seven

The metrics MAE, RMSE and MPE were calculated on the temperature data, and they are presented in table 5.4. The MAE is largest for "Side 1 - In" and "Side 2 - Out" (3.05 K and 2.67 K). The difference between the RMSE and MAE is much larger for "Side 2 - In" than any other port, indicating that that sensor had a larger variance. See for example the two local minima (valleys) located just before the end of session six in figure 5.13c.

TABLE 5.4: Temperature metrics from the in-house kit

Port	MAE (K)	RMSE (K)	MPE (%)
Side 1 - In	3.05	3.48	6.03
Side 1 - Out	1.14	1.56	2.18
Side 2 - In	1.64	2.69	0.63
Side 2 - Out	2.67	3.12	7.04

The pressure drop measurements by the in-house kit fit the true values very well as seen in figure 5.14. On side 1, the underestimation is higher at higher pressure drops indicating that the scaling is a bit too low. On side 2, the same behaviour is noticed but there is also a constant offset that needs to be calibrated for.

The behaviour that stands out the most is the values coming from the thermal rig (purple) at the beginning of session six and seven on side 1, see figure 5.14a. The thermal rig measures a lower pressure drop compared to the in-house sensors, the pressure drop from the thermal rig then increases linearly until a certain point where the signal flattens out.

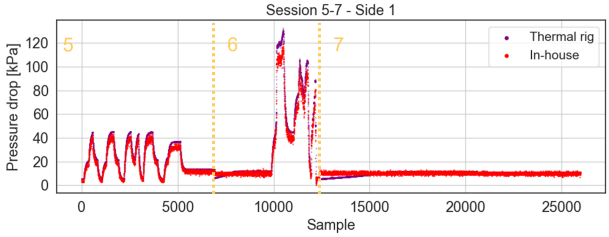

(A)

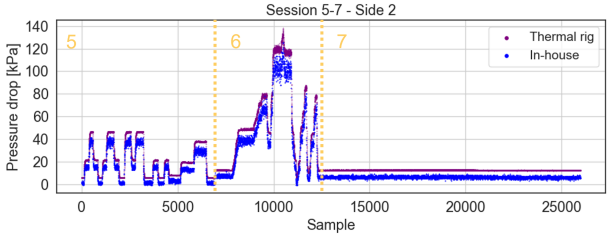

(B)

FIGURE 5.14: Shows the pressure drop data collected from the in-house kit and thermal rig during sessions 5–7

Chapter 6

Discussion

This chapter involves the analysis and discussion of the results, divided into three distinct sections, corresponding to each sensor type. In addition to presenting the findings, the chapter also covers an exploration of future opportunities and limitations associated with the study.

6.1 Flow switch

The flow switch performs quite well in the sense that it generally follows the same curve as the true flow and gives a relatively small error. During the testing, two issues were noticed.

The sensor sometimes experiences output "jumps", sudden changes in output not aligned with the true flow and without any obvious cause. This behaviour was noticed during session six, where the flow output suddenly dropped from 15 l/s to approximately 7 l/s. The sensor did not correct itself as time progressed. The fault could have been caused by a mechanical event such as the flow switch moving slightly out of the pipe or an electric event where one of the cables malfunctioned. Since the behaviour was only observed during session six the flow switch generally performed well. Therefore, more testing has to be done to see how recurrent the issue is and to identify any potential cause and consequently fix it.

Apart from the sudden "jumps" in flow output, an interesting behaviour of the flow switch was spotted, the output is sensitive to the

temperature. It increases with the temperature and the effect seems to be larger at high flow rates than at low. To compensate for this behaviour three regression models were set up with the second and third models including the temperature.

6.1.1 Calibration and temperature compensation

Since the goal of this thesis is to evaluate methods of measuring the flow for GPHEs sold to customers, it is important that the method works for a large assortment of GPHEs. For instance, any model used to improve the accuracy of the flow measurement should be generalizable. Since the flow switch was only tested with two types of GPHEs in this thesis, the focus when developing the model was on inference not prediction. Thus, simple and multiple linear regression were chosen. The models are easy to implement and easy to interpret.

The simple regression fitted the measured value to the true value with an R-squared value of 0.969. The absence of the temperature in the model meant that errors caused by temperature remained, the model thus served as a simple calibration. Model 2 improved the fit substantially but some errors were still present. When examining the results, the temperature dependence seemed to be higher at high flow rates than low flow rates, see for example the second "valley" in session two, presented in figure 5.7a. There, the temperature increases substantially with time but there is next to no increase in the measured flow rate. Compare that to the measured peaks in the same graph, these show strong indications of a correlation between flow and temperature. This observation led to the introduction of the third model, multiple regression with an interaction term which proved even better with the lowest MAE, RMSE and MAPE. Note that the metrics are calculated based on the whole dataset. If the dataset had been evenly distributed in regards to the volume flow rate the errors corrected by the interaction term could potentially have a larger effect on the metrics. Thus, seeing an improvement in the model performance even without distributed data is a good indicator of the model's performance.

Since the flow switch works on a calorimetric principle, using the temperature to read the flow, the temperature dependency was not expected. It was assumed that the flow switch would be able to compensate for the temperature dependency by itself. If this sensor is to be installed in GPHEs, compensating for the temperature dependence could be an important way of increasing the accuracy of data needed for the service offering, such as the time until maintenance. The models introduced in this thesis could serve as a baseline for future models. These models will have to be robust if they are to be used on a wider scale, thus it is important to properly understand the mechanics behind the temperature dependency. After much reasoning and discussion, an obvious cause of the issue could not be decided on.

Hopefully, if the "jump" and calibration issues can be solved, these models will prove valuable in improving the accuracy of the flow switch and enable a future service offering which includes direct flow measurements.

The flow switch has only one analogue output. From this output, the flow or the temperature can be selected with the flow being the default. The flow switch can, however, be digitally connected using IO-link instead. IO-link is a communication standard purposely made for short-distance communication with sensors and actuators (Heynicke et al., 2018). By using IO-link, the flow switch could output both the flow and temperature. The temperature could, potentially, be used to improve the accuracy of the flow switch using similar models as presented in this study. Using the temperature measured by the flow switch itself as input to the model could be more robust since the temperature is used to calculate the flow. However, using the temperature from the sticker sensors or in-house sensors could be a cheaper solution since the temperature measurements from the flow switch would not be needed and therefore not the IO-link either. Before putting the flow switch through further testing it could be beneficial to contact the supplier to see if they can give any insight into the problems evident from this thesis.

6.2 Sticker sensor kit

The sticker sensors, on average, measure a lower temperature than the reference value. There are three possible reasons for the temperature difference measured. The sticker sensors are not in direct contact with the media. The media and sensors are separated by a plate and the adhesive part of the sticker sensor. Thus, the sensors might be cooled down enough by the ambient air to create this difference. Since the temperature on side 2 is closer to the ambient temperature the error on side 2 was expected to be lower, if the ambient temperature was the cause of the error. However, this was not the case, the MAE was higher for the outlet on side 2 than side 1.

The most apparent conclusion that can be made from the metrics is that the inlet sensors have larger measurement errors than the outlet sensors. The cause for this discrepancy is not known. It could be a matter of chance. One sensor could be calibrated better than another. It could also be caused by the installation procedure, imagine one sensor with a chunk more adhesive than another, if the adhesive has poor thermal conductivity it could potentially have an impact on the result.

Considering the relatively small errors the sticker sensors still perform quite well. Especially compared to the in-house kits raw data.

6.3 In-house kit

The in-house kit exhibits both lag and a constant underestimation for three out of four sensors tested. This underestimation is most likely the cause of the installation of the sensors. All sensors are installed on the connectors (during sessions 5–7). The sensors are not completely isolated from the surroundings. The ambient air could affect the temperature of the sensors together with the connectors themselves which, due to their thickness, can take up a lot of heat. The proximity to the connectors could mean that the connectors cause thermal inertia of the in-house sensors, contributing to the lag which was shown. The effect from the ambient air could be the cause behind the underestimation, an indication that this is true is that the sensor

least affected by the underestimation is the one located on the input on the cold side (side 2). The difference between the temperature and the ambient air is the lowest in that position and will therefore have a lesser effect than on the other sensors.

The potential issues that these errors can cause are dependent on how the sensors will be used. If the sensors will be used with a high temporal resolution, the lag could cause measurement errors that can not be ignored. If the temporal resolution is of less concern, the lag could safely be ignored. The other issue, constant underestimation, is not dependent on the temporal resolution. It is therefore important to come up with a way to correct for the underestimation without calibration on every GPHE it is installed on. As mentioned in chapter 3, there is an existing model that needs to be updated based on the new installation method. The data collected in this thesis could be used for that purpose.

Chapter 7

Conclusion

In this thesis, the research objectives were to evaluate an inexpensive flow switch, a sticker sensor kit and an in-house kit with the purpose of improving Alfa Laval's service capabilities.

The flow switch performs quite well with only small errors generally. During the testing, two issues were noticed. Sudden "jumps" in the output and a temperature dependency. The temperature dependency could be compensated for by using multiple regression while the cause of the "jumps" is yet unknown. The sticker sensors' temperature measurements have good accuracy. However, the sticker sensors are also made to provide pressure data that in turn might be used to model the flow. Moving forward, more tests will be needed for the calibration of the pressure measurements. When the calibration is finished, additional experiments can be performed with the goal of modelling the flow using, the sticker sensor data and possibly also the data from the in-house kit. The in-house kit works quite well when the time resolution is low, otherwise lag affects the results, possibly due to thermal inertia. In the future, it would be interesting to see if it is possible to improve the accuracy of the in-house kit by constructing a calibration model taking the surrounding material effect on the sensor into account.

In conclusion, the thesis has provided valuable insight into the performance of the evaluated sensors, which will drive Alfa Laval's advancement towards improved service capabilities.

Bibliography

(1) Batchelor, C. K.; Batchelor, G. K., *An introduction to fluid dynamics*; Cambridge university press: 1967.

(2) Brown, G. O. In *Environmental and water resources history*, 2003, pp 34–43.

(3) Guo, B.; Ghalambor, A., *Natural gas engineering handbook*; Elsevier: 2014.

(4) Hanke, J. E.; Wichern, D. W., *Business Forecasting: Pearson New International Edition*; Pearson Higher Ed: 2013.

(5) Hewitt, G. F.; Shires, G. L.; Bott, T, *Process heat transfer*; Begell House: 1994.

(6) Heynicke, R.; Krush, D.; Cammin, C.; Scholl, G.; Kaercher, B.; Ritter, J.; Gaggero, P.; Rentschler, M. *Journal of Sensors and Sensor Systems* **2018**, *7*, 131–142.

(7) James, G.; Witten, D.; Hastie, T.; Tibshirani, R., *An Introduction to Statistical Learning: with Applications in R*; Springer Nature: 2021.

(8) Laval, A. How GPHEs work | Alfa Laval `https://www.alfalaval.com/microsites/gphe/tools/how-gphes-work/`.

(9) Lee, W.-M., *Python machine learning*; John Wiley & Sons: 2019.

(10) Qin, R.; Duan, C. In *Journal of Physics: Conference Series*, 2017; Vol. 916, p 012038.

(11) Sundén, B.; Manglik, R. M., *Plate heat exchangers: design, applications and performance*; Wit Press: 2007; Vol. 11.

(12) Willmott, C. J.; Matsuura, K. *Climate research* **2005**, *30*, 79–82.